Towards Unified Probabilistic Rotorcraft Damage Detection and Quantification via Non-parametric Time Series and Gaussian Process Models

Ahmad Amer
PhD Candidate
Center for Mobility with Vertical Lift (MOVE)
Rensselaer Polytechnic Institute, Troy, NY, USA

Fotis Kopsaftopoulos
Assistant Professor
Center for Mobility with Vertical Lift (MOVE)
Rensselaer Polytechnic Institute, Troy, NY, USA

ABSTRACT

The complex dynamics of rotorcraft structures under varying operational and environmental conditions demand the development of accurate and robust-to-uncertainties structural health monitoring (SHM) approaches. The inherent uncertainty within monitoring data makes it difficult for conventional methods to accurately and robustly detect and quantify damage without the need for a large number of data sets. In addition, due to the time-varying nature of rotorcraft operations, such conventional metrics might still fail even with abundance of data. In this paper, we propose a unified probabilistic damage detection and quantification framework for active-sensing, guided-wave SHM that focuses on monitoring rotorcraft structural "hotspots". The proposed framework involves three stages: The first stage incorporates statistical damage detection based on stochastic non-parametric time series (NP-TS) models of ultrasonic wave propagation signals within a hotspot sensor network configuration. The second stage involves the statistical path selection, where a NP-TS representation is used for the sole purpose of identifying damage-intersecting signal (wave propagation) paths, that is the paths that are most sensitive to damage, in order to use them in the subsequent damage quantification stage. That last stage achieves probabilistic damage quantification, where the results of the NP-TS models are used to train Bayesian Gaussian Process regression and classification models. This unified framework ensures accurate and robust damage detection and quantification in a data-efficient manner since only damage-intersecting paths are selected and used in the analysis. The performance of the proposed framework is compared to that of conventional state-of-the-art damage indices (DIs) in detecting and quantifying simulated damage in two representative coupons: a Carbon Fiber Reinforced Polymer (CFRP) coupon and a stiffened aluminum (Al) panel. It is shown that the proposed framework outperforms conventional DI-based active-sensing guided-wave SHM methods.

INTRODUCTION

In today's urban air mobility (UAM) "revolution", safety is one of the most challenging barriers to the adoption of many of the designs being proposed. The notion of eVTOL systems falling from the skies in an urban environment is simply too alarming. In this context, the Health and Usage Monitoring (HUMS) community is pushing the boundaries in order to develop more accurate and more robust, online Structural Health Monitoring (SHM) tools and systems that can ensure the safety of passengers and pedestrians alike. On a rotorcraft, this task is a complex one owing to the time-varying and nonlinear nature of structural dynamic responses (Refs. 1, 2), as well as complex failure modes that can be easily masked by the effects of varying operating and environmental states in the face of uncertainty (Refs. 3–5). Thus, there lies a need for the development of active-sensing SHM methods, where proper understanding, modeling, and analysis of stochastic structural responses under varying states and damage characteristics is achieved for clearing the road towards enabling the fully-automated, online monitoring of rotorcraft structural health and condition-based maintenance policies.

To this end, Health/Damage Indices (H/DIs) have been an integral part of any SHM/HUM system, in which some features of the signal for an unknown structural state are compared to that coming from the healthy structure (Refs. 6, 7). The most-widely used DI approaches are based on the time delay of specific modes in the acousto-ultrasound signal, the amplitude/magnitude of the signal, and the energy content of the signals, all used as the features for damage detection (Refs. 3, 6–10) and quantification (Refs. 11–14). These approaches, thereon denoted as conventional DI-based methods, have been used extensively owing to their simplicity, as well as the damage-no damage paradigm entertained by this analysis tool, which facilitates decision-making by maintainers on the ground (Ref. 8). However, there exists a number of challenges these types of methods are facing when it comes to damage detection. Mainly, the aforementioned issues (lack of robustness to uncertainties and applicability to complex structures) form the most compelling challenges facing the conventional DI-based approaches for damage detection (Refs. 1, 4, 5, 15–18).

Presented at the VFS International 76th Annual Forum & Technology Display, Virginia Beach, Virginia, October 6–8, 2020.

In addition, the need for user-defined damage thresholds for damage detection (Refs. 19, 20), and the phenomenon of saturation (Ref. 21) are also two major challenges faced by such methods. As such, there has been a plethora of research endeavors during the last decade aiming to enhance the detection and quantification abilities of conventional DI-based methods, as well as propose new metrics for damage detection and quantification. For damage detection, some of the most common approaches enhance current time-domain DIs by adding physics-based terms into the DI formulation, such as terms that depend solely on guided-wave propagation coefficients (see for instance (Refs. 3, 22)). Other approaches use frequency-domain or mixed-domain DIs, which exhibit better damage detection performance compared to conventional DIs (see for instance (Refs. 8, 19, 23)). Both of these strategies are, however, not probabilistic in nature, and are thus still prone to significant errors due to various sources of uncertainty. Another family of "enhanced" DI-based methods is based on baseline-free techniques, which show increased robustness to varying conditions owing to the lack of pre-sampled baseline signals (see (Refs. 20, 24)). However, they oftentimes require knowledge of dispersion curves for the components being monitored and dictate sophisticated actuation strategies. In addition, it has been shown that, depending on the actuator-sensor path from which the signal is coming, the evolution of the DIs can proceed in a manner uncorrelated with damage evolution (Refs. 8, 25), which clearly limits the applicability of many of these techniques to specific sensor network designs and simple boundary conditions. Although there are recent studies on averting this latter drawback (Refs. 26, 27), these approaches still require significant user experience in defining detection thresholds.

For damage quantification, due to the drawbacks of the DI approach outlined above, many researchers turned their attention to advanced signal processing techniques in order to quantify damage in an active-sensing framework (see (Refs. 28–33)), such as the wavelet and Hilbert-Huang transforms. While all of these techniques indeed show superiority to approaches utilizing DIs, they still lack the proper determination of quantification confidence bounds, and are thus not suitable for stochastic systems without further development. Other quantification approaches in the literature of active-sensing guided-wave SHM involve the use of analytical guided-wave models; see for instance (Refs. 34–36).

Because of the drawbacks of the aforementioned approaches, many researchers have proposed the use of statistical and/or probabilistic methods in devising active-sensing SHM method (for instance see (Refs. 37–46) for probabilistic and/or statistical damage detection and localization, as well as (Refs. 25, 37, 47–49) for damage quantification). The words *probabilistic* and/or *statistical* are used here because these techniques involve the application of probabilistic/statistical modelling approaches (such as Gaussian Mixture Models (Ref. 19)), and statistical inference techniques (such as statistical hypothesis tests (Ref. 43)). In general, these techniques lead to an accurate and robust damage quantification process (same can be said for detection). However, they may involve complicated steps (such as the case of Gaussian mixture models (Ref. 19)) or require many data sets for model training and building processes (such as the case of the matching pursuit decomposition (Ref. 30) or Bayesian updating (Ref. 48)).

In this work, a novel, unified probabilistic framework for damage detection and quantification is proposed within active-sensing acousto-ultrasound SHM and applied to two experimental test cases related to rotorcraft structural components. Stochastic, non-parametric time series (NP-TS) representations are proposed for detecting damage, as well as identifying the wave propagation paths (within a "hotspot" configuration) that are most sensitive to damage and enable robust damage detection. Then, these damage-information-rich signal paths are used to enable the statistical learning phase of the proposed unified damage detection and quantification framework *via* the use of Bayesian Gaussian Process Regression or Classification Models (GPRMs or GPCMs). The proposed framework is applied to a stiffened aluminum (Al) panel and a carbon fiber-reinforced polymer (CFRP) coupon, both representing parts of rotorcraft fuselage, within an active-sensing, local "hotspot" monitoring configuration. Experimental results are compared with one state-of-the-art DI formulation as proposed by Janapati *et al.* (Ref. 3) and Qiu *et al.* (Ref. 19). The novel aspects of this work include:

(a) The introduction of a unified probabilistic SHM framework for damage detection and quantification, and its experimental demonstration to both metallic and composite coupons representing rotorcraft structural components.

(b) The development of a novel straight-forward damage detection tool in active-sensing guided-wave SHM with the advantage of enhanced detection capabilities over conventional DI-based approaches, without sacrificing simplicity.

(c) The integration of the NP-TS model results into GPRMs and GPCMs for enhanced accuracy and robustness in damage quantification and classification, respectively.

(d) The extraction of statistical confidence intervals for damage detection and quantification from the response signals of piezoelectric sensors directly, negating the requirement of user-defined thresholds.

THE UNIFIED STATISTICAL DAMAGE DETECTION AND QUANTIFICATION FRAMEWORK

A unified probabilistic SHM framework is proposed integrating stochastic NP-TS representations with GPRMs and GPCMs for damage detection, quantification and classification. Figure 1 shows the flow chart of the proposed workframe. As shown, in the "training phase," training data is first acquired, and all signals from all actuator-sensor paths are fed into NP-TS models. These models perform the detection, as well as provide certain data features that are fed

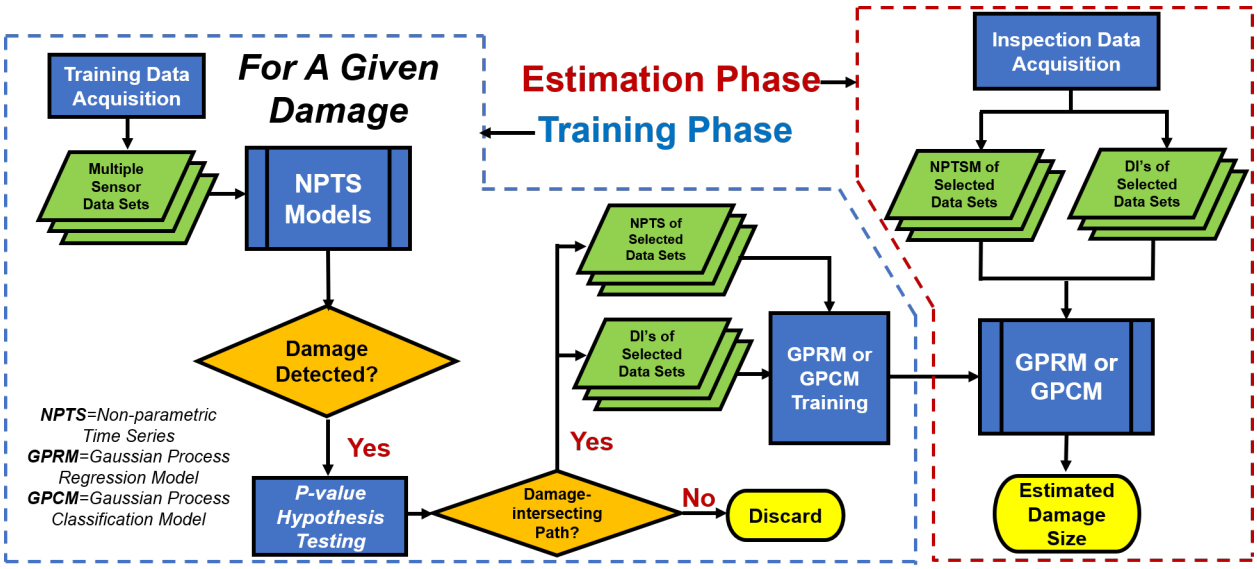

Fig. 1. The proposed unified framework integrating NP-TS representations with GPRMs and GPCMs for probabilistic damage detection and quantification in active-sensing guided-wave SHM.

into a statistical path selection algorithm to classify paths into damage-intersecting and non-intersecting according to properly-selected statistical quantities (p-values). After that, the DIs and the NP-TS representations of only those damage intersecting paths are used to train GPRMs or GPCMs for damage quantification.

Then, in the "estimation phase," inspection data is collected and the DIs and/or the NP representations of the selected signal paths are extracted and fed into the trained GPRMs/GPCMs, from which the most probable damage size is extracted, thus fulfilling both the detection and quantification within a unified probabilistic SHM framework. In a recent study by the authors (Ref. 43), the statistical path selection framework has been demonstrated on an Al plate and the stiffened Al panel used herein, and thus, although the theoretical background of statistical path selection will be presented, results of applying the framework will not be presented here for the sake of brevity. In addition, integrating the DIs of the selected signal paths for damage quantification has also been previously presented by the authors (Ref. 25), so in this study, results will be presented only for the integration between NP-TS and GPR/GPC models.

Statistical Damage Detection

Kopsaftopoulos and co-workers (Refs. 50–52) have previously reported a statistical framework for damage detection and identification for vibration-based SHM, which was later expanded by the authors in the context of active-sensing guided-wave SHM (Ref. 43). For the purpose of damage detection, quantification and localization, this framework can be laid out as shown in Figure 2 (Refs. 43, 53), where $x[t]$ and $y[t]$ are the actuation and response signals, respectively. These signals are indexed with discrete time t, which corresponds to continuous time $(t-1)T_s$, where T_s is the sampling time for the recorded data. The subscripts $(o, A, B, \ldots,$ and $u)$ indicate the healthy, damage A, B, ..., and unknown cases, respectively. The different damage labels $(A, B, \ldots)$ can represent different sizes, types, or locations of damage. For each structural state, all actuation (X) and response (Y) signals can be presented as $Z = (X, Y)$, with $Z_o, Z_A, Z_B, \ldots,$ and Z_u indicating the different states as before.

Figure 2 shows two phases in this framework: a baseline and an inspection phase. In the latter, the identification and validation of NP-TS models is carried out for producing a characteristic quantity $\widehat{Q}$ for the healthy $(\widehat{Q}_0)$ and the different predefined damage states $(\widehat{Q}_A, \widehat{Q}_B, \ldots)$. In the inspection phase, applying the developed NP-TS models for the unknown state, the quantity $(\widehat{Q}_u)$ is identified for the system. Damage detection and identification (quantification and/or localization) can then be carried out by applying binary statistical hypothesis tests, where the statistical deviation of $\widehat{Q}_u$ from $\widehat{Q}_0$ (damage detection) and its statistical similarity thereof to one of the damaged state quantities: $\widehat{Q}_A$, $\widehat{Q}_B, \ldots$ (damage identification/classification) is interrogated. In this study, this framework is only used for damage detection, while GPRMs/GPCMs are used for damage quantification. Finally, it is worth noting that, although binary hypothesis tests are based on the type I (α) and II (β) error probabilities, only the former can be defined for the framework applied herein (Ref. 54).

The Welch Non-parametric Time Series Representation. Because of their stochastic nature, NP-TS models have been extensively utilized in the field of vibration-based SHM (Refs. 52, 55, 56). Their main advantage lies in the straightforward statistical representation of theoretical and experimental estimation uncertainties, which removes the need for user-defined damage thresholds. In addition, application of these models requires little-to-no user experience (Refs. 57,

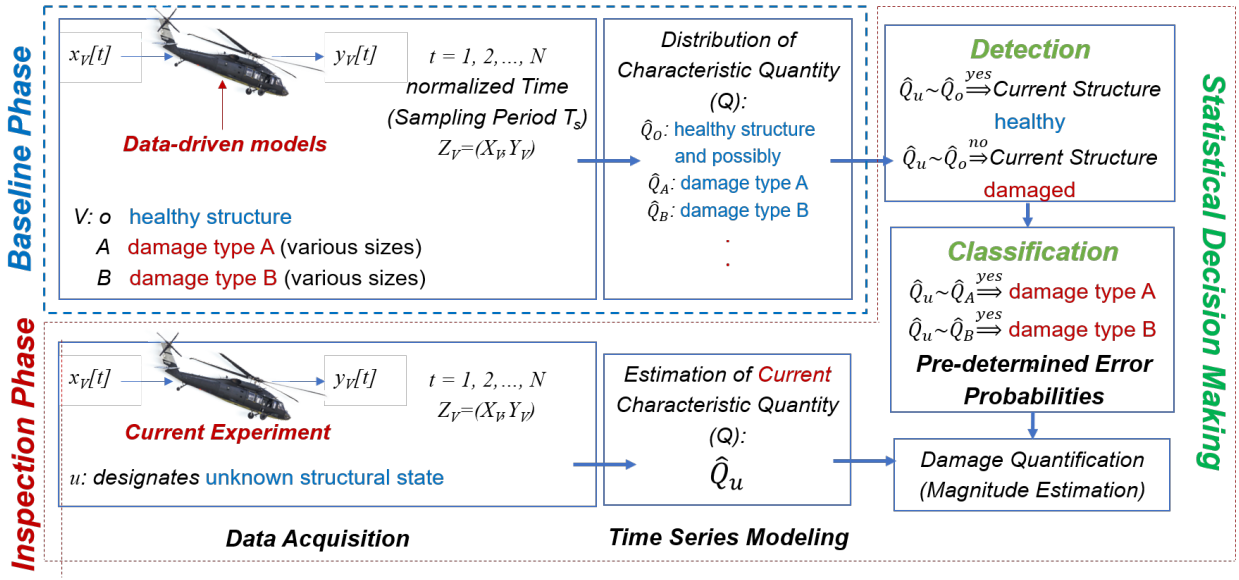

Fig. 2. Framework for statistical time series methods for structural health monitoring (Refs. 43, 52, 53).

58). Finally, as will be shown herein, NP-TS models can prove superior to DI-based approaches in following damage evolution. Some of the most widely-used NP-TS models are estimators for the Power Spectral Density (PSD) of a sensor response signal (Refs. 57–59). The term "estimators" is used here because the signals used in the estimation are finite in nature, making such representations estimators of the true PSD of a system. In this study, the Welch-based PSD estimator (also known as the Barttlet-Welch estimator) (Ref. 58, Chapter 4, pp. 76) is used for damage detection. For a time series signal $x[t]$, the frequency-domain (ω) Welch-based PSD ($\widehat{S}_{xx}(\omega)$, or $\widehat{S}(\omega)$) is based on the averaging of multiple-windowed periodograms using properly-selected sample windows $w[\tau]$ with 50% overlap, and is calculated as follows (Refs. 60, 61) (the hat indicates an estimated quantity):

$$\widehat{S}_{xx}(\omega) = \frac{1}{KLUT} \sum_{i=0}^{K-1} \left| T \sum_{t=0}^{L-1} w[t] \cdot \widehat{x}[t+iD]^{(-j2\pi\omega tT)} \right|^2 \quad (1)$$

with

$$U = \frac{1}{L} \sum_{t=0}^{L-1} w^2[t], \quad \widehat{x}[t] = x[t] - \widehat{\mu}_x, \quad N = L + D(K-1) \quad (2)$$

and N, L, K, D, and T being the total number of signal samples, the size of each window, the number of utilized windows, the number of overlapping data points in each window, and the time period of the signal, respectively. $\widehat{\mu}_x$ represents the mean of the time series, and $|\cdot|$ represents the Euclidean norm. The estimation statistics, that is the mean and variance, of the Welch PSD can be described as follows:

$$E\{\widehat{S}_{xx}(\omega)\} = \frac{1}{2\pi LU} S_{xx}(\omega) |W(\omega)|^2 \quad (3)$$

$$Var[\widehat{S}_{xx}(\omega)] = \frac{9}{16} \frac{L}{N} S_{xx}^2(\omega) \quad (4)$$

where $W(\omega)$ is the Fourier transform of the window function. One of the main reasons behind the wide use of the Welch PSD estimator is that it is asymptotically unbiased and consistent (Ref. 59).

The Multiple-set Z Statistic. As presented in the work of Kopsaftopoulos and Fassois (Refs. 52, 53), changes in the Welch-based PSD of time series signals can be indicative of structural damage. In real-life situations, there would generally be a sufficiently-large number of data sets for the healthy/baseline case. In that case, the mean of the multiple Welch PSD estimators of the multiple available signals can be assumed to approximately follow a normal distribution (Refs. 52, 53). In this study, we develop a novel damage detection statistical quantity based on the Z statistic developed by Kopsaftopoulos and Fassois (Refs. 52, 53). The novelty here stems from the utilization of the mean of the estimators, instead of the estimators themselves, as well as the use of the Welch PSD estimator instead of the FRF. Herein, this novel Z statistic is used, for the first time, for analyzing active-sensing acousto-ultrasound SHM signals. Then, damage detection can be tackled using the following SHT problem:

$$\begin{aligned} H_o &: E\{S_o(\omega)\} - S_u(\omega) = 0 \\ &\quad \text{(null hypothesis – healthy structure)} \\ H_1 &: E\{S_o(\omega)\} - S_u(\omega) \neq 0 \\ &\quad \text{(alternative hypothesis – damaged structure)} \end{aligned} \quad (5)$$

In this formulation, $S_u(\omega)$ represents the PSD of the unknown structural case. Using the property of mutual-independence between the time series of the healthy and damage structures, the PSD estimates for these states would also be mutually-independent, along with the differences between these estimates (that is $E[\widehat{S}_o(\omega)] - \widehat{S}_u(\omega)$). In the latter case, the distribution of the differences would have a mean equal to the

difference between the true PSD estimates, and a variance equalling the sum of both variances (the variance of $E[\widehat{S}_o(\omega)]$ and $\widehat{S}_u(\omega)$). Finally, the null hypothesis can be set up as follows:

$$\begin{gathered}\text{Under } H_o: E\{\widehat{S}_o(\omega)\} - \widehat{S}_u(\omega) \sim \mathcal{N}(0, 2\sigma_o^2(\omega)) \\ \text{(null hypothesis – healthy structure)}\end{gathered} \tag{6}$$

Here, σ_o^2 can be estimated from the baseline phase, and can be assumed to have negligible variability for a large number of data sets (Refs. 52, 53). The Welch PSD-based Z statistic can be expressed as follows:

$$\begin{aligned} Z = \frac{|E\{\widehat{S}_o(\omega)\} - \widehat{S}_u(\omega)|}{\sqrt{2\sigma_o^2(\omega)}} \leq Z_{1-\frac{\alpha}{2}} \quad (\forall\, \omega) \quad &\Longrightarrow \quad H_o \text{ is accepted} \\ \text{Else} \quad &\Longrightarrow \quad H_1 \text{ is accepted} \end{aligned}$$

where $Z_{1-\frac{\alpha}{2}}$ designating the standard Normal distribution's $1-\frac{\alpha}{2}$ critical point.

Reference Damage Index. In this work, a reference state-of-the-art DI was adopted from the work of Janapati *et al.* (Ref. 3). This specific formulation was selected because it is characterized by high sensitivity to damage-related characteristics (such as size and orientation) *vs* other sources of signal variations (such as material properties). Given a healthy $x_o[t]$ and an unknown $x_u[t]$ signal, the formulation of the selected DI is as follows:

$$N_u = \frac{x_u[t]}{\sqrt{\sum_{t=1}^{n} x_u^2[t]}}, \tag{7a}$$

$$N_0 = \frac{\sum_{t=1}^{n}(x_o[t] \cdot N_u)}{x_o[t] \cdot \sum_{t=1}^{n} x_o^2[t]} \tag{7b}$$

$$DI = \sum_{t=1}^{n}(N_u - N_o) \tag{7c}$$

In equation 7c, N_u and N_o are normalized unknown- and baseline-case signals, respectively.

Probabilistic Damage Quantification

As described above, the proposed framework (Figure 1) involves both damage detection and quantification. NP-TS representations of the response signals of different actuator-sensor paths are fed into a statistical path selection algorithm, which identifies signal paths as damage-intersecting or damage-non-intersecting based on statistical quantities. After that, the NP-TS representations of only the damage-intersecting paths are used to train GPRMs/GPCMs for damage size estimation, as shown in Figure 1. As previously reported (Refs. 25, 43), damage-intersecting paths carry more information about damage size compared to non-intersecting paths. Thus, only using these paths in training GPRMs/GPCMs would greatly decrease the amount of data sets required for accurate damage quantification. This is is achieved by using the proposed statistical path selection approach.

Statistical Path Selection. A different, but similar, algorithm to compute the PSD involves the use of a sliding window with overlap exceeding 50%, which gives PSD results that are both frequency- and time-dependant. This algorithm is the Short-Time Fourier Transform (STFT), and, written in a form similar to the Welch PSD estimation, it can be applied as follows:

$$\widehat{S}_{xx}(\omega,\tau) = \frac{1}{KLUT}\sum_{i=0}^{K-1}|T\sum_{n=0}^{L-1} w[n-\tau]\widehat{x}[n+iD]e^{-j2\pi\omega nT}|^2$$

In this work, the STFT PSD is used as a damage-sensitive feature to identify which actuator-sensor signal paths intersect damage and which do not. In order to implement this statistical path selection process, the STFT PSD estimates are fed into another statistical hypothesis test, namely the Kolmogorov-Smirnoff (KS) test. The KS test was originally proposed as a means for measuring the deviation of an empirical distribution from a theoretical one (Refs. 62–64). The on-sided two-sample version of the KS statistic of the test can be calculated as follows (Refs. 64, 65):

$$KS_{nn'} = \sqrt{\frac{nn'}{n+n'}}\, sup_x(F(\widehat{S}_o(\omega,\tau)) - F(\widehat{S}_u(\omega,\tau))) \tag{8}$$

Here, F indicates the empirical cumulative distribution function (CDF) of the STFT PSD time samples of the healthy and the unknown cases being compared having sizes n and n' (in this work, n is equal to n'). $sup_x(\cdot)$ indicates the supermum of the enclosed quantity, and $\widehat{S}_o(\omega,\tau)$ and $\widehat{S}_u(\omega,\tau)$ are the STFT PSD estimates for the healthy and unknown case, respectively. In this case, if $KS_{nn'}$ is larger than a critical value KS_α defined by a selected false alarm level α. Tables for the critical values of KS_α can be found in (Ref. 66). An alternative way of reaching a decision would be to compare the p-values of having $KS_{nn'}$ either being positive or negative (Ref. 65). Some of the advantages of the two-sample KS test include applicability to small sample sizes and to samples where the difference in distributions is small (Ref. 64). Applying the two-sample KS test in this study, the empirical CDFs of the estimated STFT PSD values $\widehat{S}_{xx}(\omega,\tau)$ at different time points τ (for each value of ω) for the healthy as well as the unknown test cases are compared. Then, the p-value of having the empirical CDF of the healthy case less than that of the unknown case (that is, having a negative $KS_{nn'}$) is calculated and compared with the significance of the test (α). Based on that, a one-sided statistical hypothesis test can be setup as follows:

$$\begin{aligned} &H_o: p_u(\omega) \geq \alpha \quad \text{(damage-non-intersecting path)} \\ &H_1: p_u(\omega) < \alpha \quad \text{(damage-intersecting path)} \end{aligned}$$

such that p_u is the p-value of the one-sided two-sample KS test when the unknown STFT PSD estimate is compared to the healthy one.

Bayesian Gaussian Process Regression Models. GPRMs are kernel-based linear regression formulations that have the ability to model non-linear relationships between observations

and inputs. In this study, GPRMs are used to model the evolution of the Z statistic with frequency and/or damage size as will be shown later. Given a training data set $\mathcal{D}$ containing n inputs-observation pairs $\{(\mathbf{x}_i \in \mathbb{R}^D, y_i \in \mathbb{R},\ i = 1,2,3,\ldots,n\}$, a GPR model can be formulated as follows:

$$y = f(\mathbf{x}) + \epsilon \tag{9}$$

such that a GP prior with mean $m(\mathbf{x})$ and kernel $k(\mathbf{x},\mathbf{x}')$ is placed on the latent function $f(\mathbf{x})$, and an independent, identically-distributed (*iid*), zero-mean Gaussian prior with variance σ_n^2 is placed on the noise term ϵ as follows:

$$f(\mathbf{x}) \sim \mathcal{GP}(m(\mathbf{x}), k(\mathbf{x},\mathbf{x}')), \quad \epsilon \sim iid\, \mathcal{N}(0,\sigma_n^2) \tag{10}$$

In this study, $m(\mathbf{x})$ is set to zero, and the squared exponential kernel function is used for f:

$$k(\mathbf{x},\mathbf{x}') = \sigma_0^2 \exp(-\frac{1}{2}(\mathbf{x}-\mathbf{x}')^T \Lambda^{-1}(\mathbf{x}-\mathbf{x}')) \tag{11}$$

where σ_0^2 is the output signal power (variance), and Λ is a diagonal matrix of the characteristic length scales of each dimension (D, i.e each covariate) in the input data set. There will be a separate length scale for every covariate in the data. Thus, for a single-input (i.e. $D = 1$), the entries along the diagonal of Λ^{-1} will be identical.

GPRM training involves optimizing the hyperparameters ($\theta \equiv \sigma_0^2, \Lambda, \sigma_n^2$) *via* Type II Maximum Likelihood (Ref. 67, Chapter 5, pp. 109). In this method, the marginal likelihood (evidence) of the training observations (outputs) is maximized with respect to the hyperparameters. For computational reasons, its negative log is minimized instead as follows:

$$\widehat{\theta} = \arg\min_{\theta}\{-\log p(\mathbf{y}|X,\theta)\} \tag{12a}$$

$$-\log p(\mathbf{y}|X,\theta) = -\log \mathcal{N}(\mathbf{y}|\mathbf{0}, K_{XX} + \sigma_n^2\mathbb{I}) \tag{12b}$$

$$= -\frac{1}{2}\mathbf{y}^T (K_{XX} + \sigma_n^2\mathbb{I})^{-1}\mathbf{y} - \frac{1}{2}\log|K_{XX} + \sigma_n^2\mathbb{I}| - \frac{n}{2}\log 2\pi \tag{12c}$$

One of the most powerful results of the assumptions in GPRMs is that a joint Gaussian distribution can be assumed between the training observations $\mathbf{y}$, and the test observation(s) (to be predicted) at the set of test inputs ($\mathbf{x}_*$) as follows:

$$\begin{bmatrix} \mathbf{y} \\ y_* \end{bmatrix} = \mathcal{N}\left[\mathbf{0}, \begin{matrix} K_{XX} + \sigma_n^2\mathbb{I} & \mathbf{k}_{X\mathbf{x}_*} \\ \mathbf{k}_{\mathbf{x}_*X} & k_{\mathbf{x}_*\mathbf{x}_*} + \sigma_n^2\mathbb{I} \end{matrix}\right] \tag{13}$$

In equation 13, K_{AB} is used as a shorthand for $K(A,B)$, and $\mathbb{I}$ is the identity matrix. The predictive distribution over the prediction $\mathbf{y}_*$ can then be defined from the properties of multivariate Gaussian distributions (Ref. 68) as follows:

$$p(y_*|\mathbf{x}_*, X, \mathbf{y}) = \mathcal{N}(\mathbb{E}\{y_*\}, \mathbb{V}\{y_*\}) \tag{14a}$$

$$\mathbb{E}\{y_*\} = \mathbf{k}_{\mathbf{x}_*X}(K_{XX} + \sigma_n^2\mathbb{I})^{-1} \tag{14b}$$

$$\mathbb{V}\{y_*\} = k_{\mathbf{x}_*\mathbf{x}_*} - \mathbf{k}_{\mathbf{x}_*X}(K_{XX} + \sigma_n^2\mathbb{I})^{-1}\mathbf{k}_{X\mathbf{x}_*} + \sigma_n^2) \tag{14c}$$

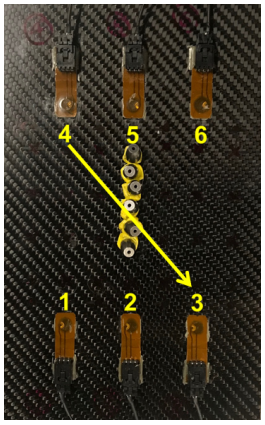

Fig. 3. The CFRP coupon used in this study shown here with 6 weights as simulated damage (largest damage size). The arrow shows the signal path used in the present work.

Bayesian Gaussian Process Classification Models. In many SHM real-life problems, classification may be an alternative to regression approach, when SHM metrics are obtained under different damage types and /or damage sizes that do not evolve in a continuous manner. This is the case with damages of discrete nature, such as rivet damages (as presented here), or multi-location impact damage (unlike for instance cracks which can be modelled using a regression framework). For these types of problems, we propose the use of Gaussian Process classification instead of regression models. Although the processes of training and prediction are very similar between GPCMs and GPRMs, there exist differences which stem from the targets (observations) being discrete labels instead of continuous observations (Ref. 67, Chapter 3, pp. 33). In the binary classification problem, this would first dictate that the latent function $f(\mathbf{x})$ be "squashed" into the domain of [01] or [−11] (Ref. 67, pp. 39). This can be done using the logistic function $\lambda(f(\mathbf{x}))$ as follows (Ref. 67, pp. 35):

$$\lambda(f(\mathbf{x})) = (1 - \exp(-f(\mathbf{x})))^{-1} = p(y = +1|\mathbf{x}) = 1 - p(y = -1|\mathbf{x}) \tag{15}$$

With this concept, prediction can take place as follows (Ref. 67, pp. 40):

$$p(f_*|X,\mathbf{y},\mathbf{x}_*) = \int p(f_*|X,\mathbf{x}_*,\mathbf{f})p(\mathbf{f}|X,\mathbf{y}) \tag{16a}$$

$$p(y_* = +1|X,\mathbf{y},\mathbf{x}_*) = \int \lambda(f_*)p(f_*|X,\mathbf{y},\mathbf{x}_*) \tag{16b}$$

In this expression, a shorthand for the latent function $f(x_*)$ and $f(\mathbf{x})$ has been introduced as f_* and $\mathbf{f}$, respectively. Also, $p(\mathbf{f}|X,\mathbf{y})$ is the posterior over the latent function. The predictive probability $p(y_* = +1|X,\mathbf{y},\mathbf{x}_*)$ allows for obtaining the probability of the test input x_* falling into the class of +1. This expression, however, cannot be solved analytically because the non-Gaussianity of the integrals in equation 16. Thus, approximate methods are used to solve the integrals by approximating the non-Gaussian posterior by a Gaussian one. The method used herein is the expectation maximization method (Ref. 67, Section 3.6).

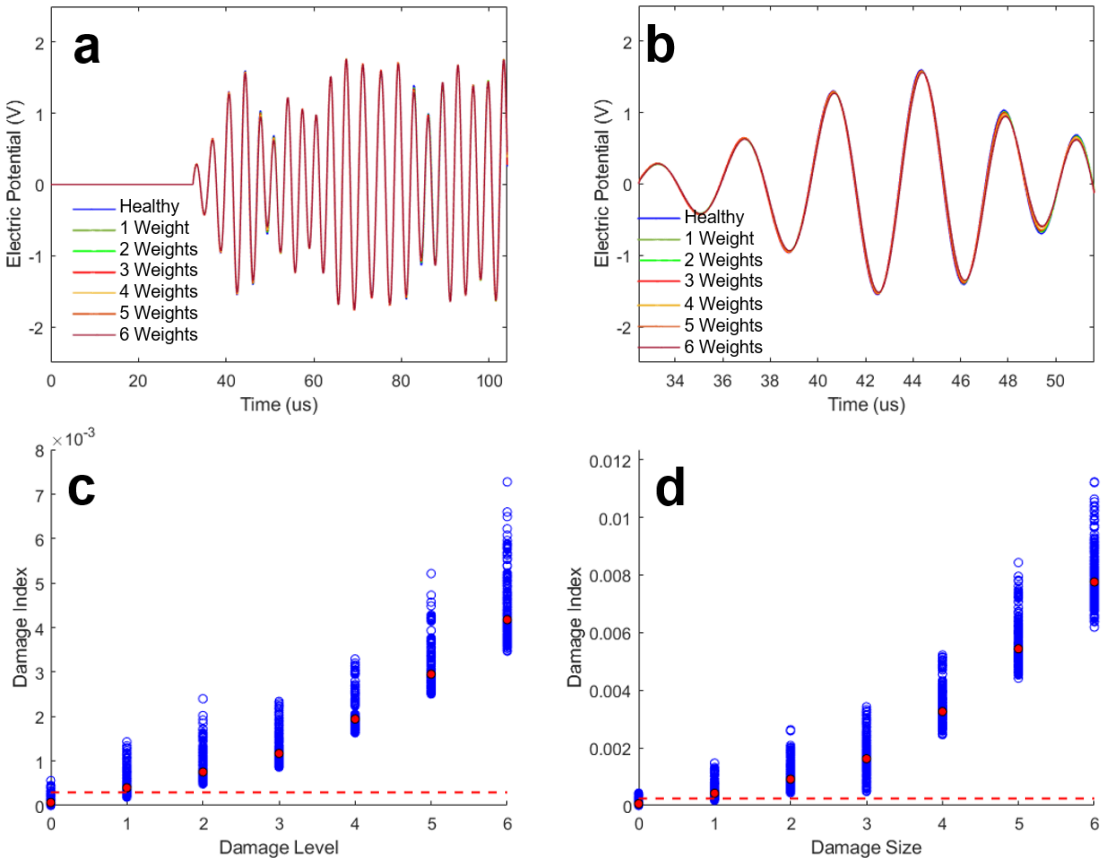

Fig. 4. Response signals from path 4-3 in the CFRP coupon and their corresponding DIs for different damage sizes (number of weights). (a) and (c) First $100\mu s$. (b) and (d) First $50\mu s$. The red dashed lines indicate the upper 95 % confidence bound for the healthy DI values, while the red circles indicate the mean of all realizations per damage.

TEST CASE 1: CFRP COUPON

Experimental Setup

In the first test case for the experimental validation and assessment of the proposed framework, a CFRP coupon was used of dimensions 152.4×254 mm (6×10 in) (2.36 mm/0.093 in thick; ACP Composites; $0/90^o$ unidirectional layup with carbon fiber prepreg). The coupon was fitted with six single-PZT (Lead Zirconate Titanate) SMART Layers type PZT-5A (Acellent Technologies, Inc) using Hysol EA 9394 adhesive, as shown in Figure 3. The PZT-5A sensors have a thickness of 0.2 mm (0.008 in) and a diameter of 3.175 mm (1/8 in). In order to simulate a growing matrix crack, up to six three-gram weights were sequentially attached to the surface of the plate using tacky tape, as shown in Figure 3.

5-peak tone bursts (5-cycle Hamming-filtered sine waves) with 90 V peak to peak amplitude and various center frequencies were generated at each sensor and the response signals at the remaining sensors were collected. Using a sampling rate of 24 MHz, 20 response signals per structural case were collected at each sensor using a ScanGenie III data acquisition system (Acellent Technologies, Inc). Preliminary analysis was conducted, and a center frequency of 250 kHz was chosen for the complete analysis presented in this study based upon the best separation between the first two wave packets in various signal paths. All analysis presented in this paper was done in Matlab.[1] For the GPRMs, the mean squared error (MSE) and the residual sum of squares divided by the sample sum of squares (RSS/SSS) are all reported with respect to the validation (test) data that was not used in the training phase.

Detection: Results and Discussion

Figure 4 shows the signals received at sensor 3 when sensor 4 was actuated under different damage cases (different numbers of attached weights), as well as the evolution of the DI. This path has been specifically chosen for analysis because it is damage-intersecting. As mentioned before, using the statistical path selection framework described in , signal paths can be identified as damage-intersecting or non-intersecting. As shown in the figure, be it for the first 50 or 100 μs, the DIs seem to follow the evolution of damage with all damages being detected with 95 % confidence, albeit with substantial overlap over different realizations. This overlap is connected

[1] Matlab version R2020a, functions *pwelch.m* (window size: 80-130; nfft: 5000; noverlap: 50%) and *spectrogram.m* (window size: 400-900; nfft: 960; noverlap: 95%).

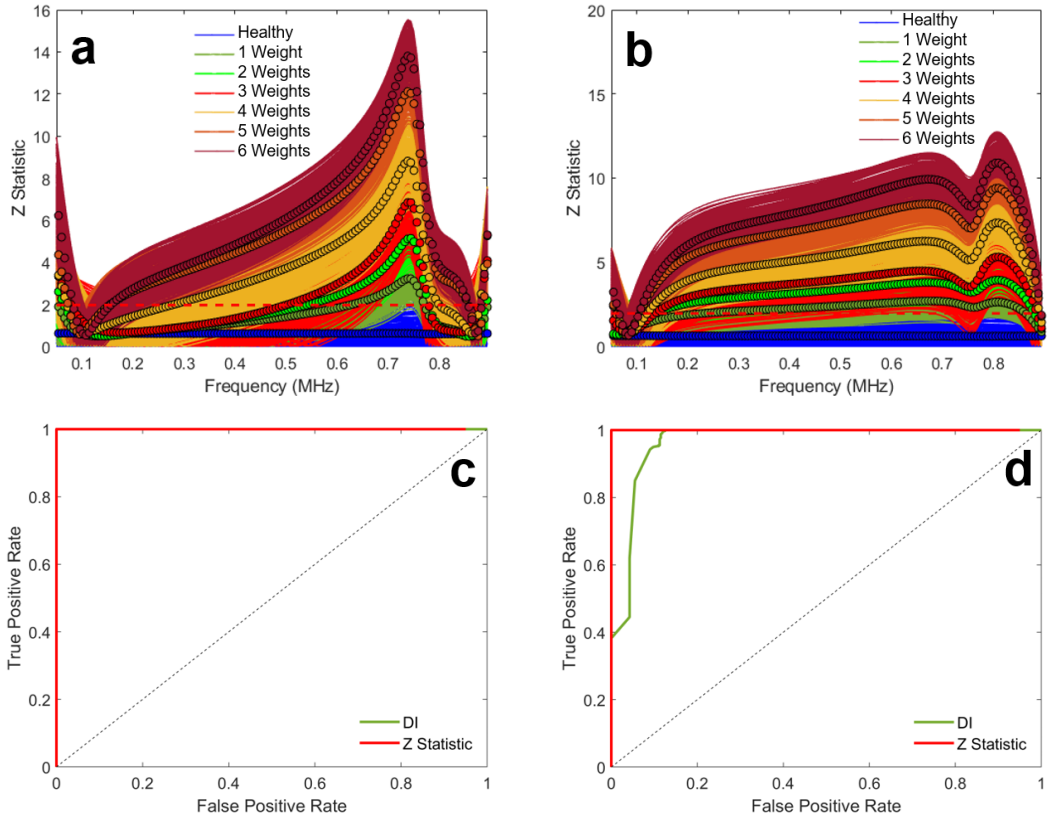

Fig. 5. NP-TS model results from path 4-3 in the CFRP coupon for different damage sizes (number of weights). (a) Z Statistic for the first $100\mu s$. (b) Z Statistic for the first $50\mu s$. The red dashed lines indicate the upper 95 % confidence bound for the healthy Z statistics, and the colored circles indicate the mean Z value of all realizations per damage. Also shown are ROC plots comparing Z statistics and DIs with respect to detecting the first damage size (1 weight) for (a) the first $100\mu s$, and the (d) first $50\mu s$.

to different sources of uncertainty affecting the different realizations/cross sections of the signals in a lab environment. Indeed, in a rotorcraft setting, this overlap would be much bigger because of the varying operational and environmental conditions, as well as the various sources of uncertainty. Although the same can be said for the challenges faced by NP-TS models in detecting damage, NP-TS models are based on statistical distributions, and thus they inherently allow for the extraction of estimation uncertainties along with experimental uncertainties. In addition, NP-TS models are defined in the frequency domain, which, as mentioned in the Introduction, offers more accuracy in detection, as well as more flexibility due to the wide spectrum of frequencies at which the analysis can be done.

Figure 5 panels a and b show the Z statistics corresponding to the signals in Figure 4. As shown, although overlap does exist between the different damage cases, especially for small damage sizes, comparing these results with the DIs, it can be observed that there are frequencies where many realizations for a given damage case are not overlapping with those of other damage cases. This can be observed by noting the position of the mean Z values, and is the case especially high frequencies in the $50\mu s$ Z statistic. Damage case-separation aside, because the main purpose of this study is comparing detection performances, ROC plots were generated for the first damage size only (one attached weight) as shown in Figure 5 panels c and d. For the first $100\mu s$ of the signal, both detection metrics show perfect damage detection, while the Z statistic shows more sensitivity in damage detection when analyzing the effect of one weight on the first $50\mu s$ of the signals. This, alongside better damage case-separation at specific frequencies, shows that the Z statistic is a promising damage detection metric compared to state-of-the-art conventional DI-based methods.

Quantification: Results and Discussion

As mentioned above, the problem of damage quantification is tackled by training GPRMs based on the generated Z statistics for the damage-intersecting paths, and then using the GPRMs for prediction. In this format, the trained GPRMs would be capable of predicting Z statistic values when given frequency and/or damage points/cases. However, because in real-life situations, test data would correspond to the SHM metric values themselves (the Z statistic in this case) instead of frequency or structural states, it would be more interesting to identify

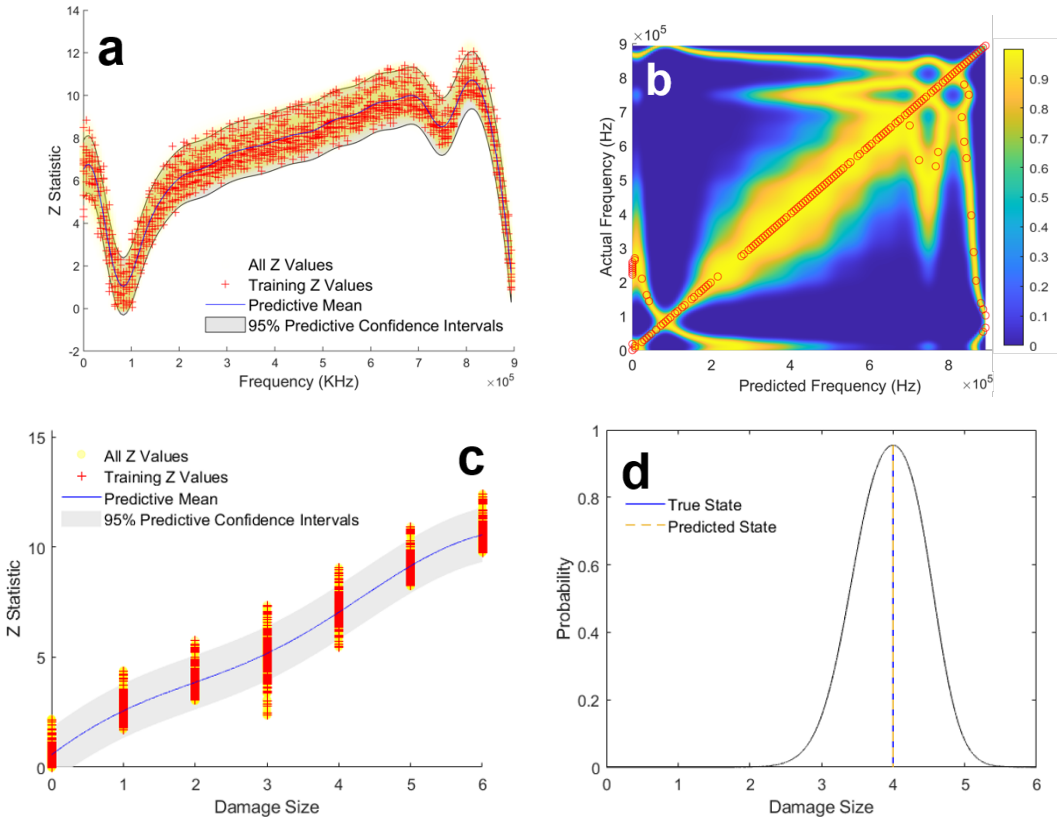

Fig. 6. GPRMs trained by Z statistic from the first $50\mu s$ of signal path 4-3 in the CFRP coupon. (a) GPRM modelling the evolution of the Z statistic with frequency for the biggest damage size (6 weights). (b) Prediction probability showing the predicted frequencies by this GPRM *vs* true frequencies. The scale bar indicates the probability, and red circles indicate the highest probability points/actual frequency. (c) GPRM modelling the evolution of the Z statistic with respect to damage size at a frequency of 792 kHz. (d) Prediction probability versus damage size based on the GPRM at an indicative test point (true and predicted states are shown as dashed vertical lines).

the frequency and/or damage size of the incoming test points using the trained GPRMs, not vice versa. This can be applied by calculating the predictive confidence intervals at the test Z statistic values, and finally calculating the probability that a point sampled from the predictive distribution of each set of states (frequency and/or damage size) would fall within the calculated confidence intervals. The state(s) that has(ve) the highest probability would be identified as the state(s) corresponding to the observed test Z statistic.

Having said that, since the Z statistics are calculated at specific frequencies, the frequency is never an unknown that needs to be predicted, unlike damage size. However, because Z statistics do change values with frequency, there exists specific frequency(ies), that have to be determined, at which Z-trained GPRMs would predict damage size most accurately. Thus, there are two methods by which this prediction problem can be approached. The first approach includes training GPRMs that model the evolution of the Z statistic with both frequency and damage at the same time, and then extracting prediction probabilities for both. This approach carries the inherent assumption that the "most-sensitive frequency" is unknown, and similar models were applied by the authors recently for aerodynamic state prediction over aircraft wings (Ref. 69). The second approach would be to generate GPRMs that only model the evolution of the Z statistic with frequency for each damage size. Then, using the frequency prediction paradigm described in the last paragraph, the frequency prediction capability of these damage-specific, Z-trained GPRMs is studied. From this, the frequency(ies) at which the damage-specific GPRMs show perfect frequency prediction across all damages (across multiple damage-specific GPRMs), that is, the "most-sensitive frequency(ies)" would be deemed as the frequency(ies) of analysis for damage quantification. Finally, the evolution of the Z statistic with damage size at one of these selected frequencies is modelled using GPRMs, from which damage size can be predicted. This second approach is the one presented here.

Figure 6a shows one such damage-specific, Z-trained GPRM that was trained using 1500 training points selected randomly from 60000 Z statistic values, but evenly-distributed over the frequency axis (MSE: 0.46, RSS/SSS = 0.76%). As shown, the model almost perfectly captures the evolution of the Z statistic with frequency, as well as the variability in the available data sets (see the yellow circles). Figure 6b shows the

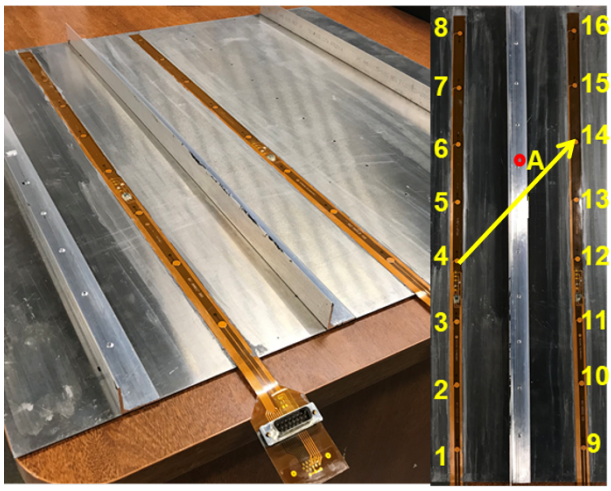

Fig. 7. The stiffened Al panel used in this study. The red circle indicates the rivet (rivet A) were damage was simulated, and the yellow arrow indicates the path analyzed in this study.

probability of the predicted frequencies *vs* the true frequencies of analysis. As shown by the circles, that indicate the location of the maximum probabilities per actual frequency, for almost the full frequency spectrum, the actual frequency is accurately predicted. Following this, similar GPRMs were trained for each of the other damage cases, and the plot shown in Figure 6b was generated for each damage case (not shown here). Observing all the similar damage-specific probability plots, a frequency of 792 kHz was chosen as the frequency at which damage quantification will be applied. Figure 6c shows the GPRM trained using all Z statistic values for all damage sizes at a frequency of 792 kHz (MSE: 0.42, RSS/SSS = 0.99%). As shown, the model nicely follows the evolution of damage in the CFRP coupon, yet still shows apparent overlap between the Z values at different damage sizes. However, unlike in the case of the DIs, where this overlap would directly affect damage quantification, the trained GPRM showed perfect damage size prediction for all Z test points that were fed into it. One example is shown in Figure 6d, where the test Z statistic point corresponds to a damage size of 4 weights. The results presented in this and the previous section show the superiority of the proposed unified framework in tackling damage detection and quantification compared to conventional DI-based approaches. It is worth noting here that, because the signal paths that are used in this analysis are statistically selected according to the framework presented in , the amount of data sets needed for training accurate GPRMs is greatly decreased compared to other quantification methods presented in the literature.

TEST CASE 2: STIFFENED AL PANEL

Experimental Setup

An 6061 Al panel having dimensions 609.6×609.6 mm (24×24 in) and being 0.81 mm (0.032 in) thick, was stiffened with three 25.4×25.4 mm (1×1 in) stringers to simulate a sub-scale fuselage component. Using Hysol EA 9394 adhesive, one 8-sensor SMART layer (Acellent Technologies, Inc) was installed at each side of one of the stringers on the panel, as shown in Figure 7. In order to simulate damage, rivet A (indicated in the figure) was subjected to three damage levels: the bottom of the rivet was completely filed (damage level 1), then rivet A was partially popped out using a hammer (damage level 2), and finally completely removed (damage level 3). Actuation and response signal collection was done in the same manner as with the CFRP plate.

Detection: Results and Discussion

Figure 8 shows the signals and DI values corresponding to signal path 4-14 under different damage levels. Just like the case of the CFRP coupon, although all damages are detected, there exists substantial overlap between the different DI values across the damage levels, more so for the first $100\mu s$ compared to the first $50\mu s$ only, in which the DI values show a more uniform evolution with damage.

Figure 9 panels a and b show the Z statistic results for the first 100 and $50\mu s$, while panels c and d show the corresponding ROC plots for the first damage level. It can be directly observed from panel a that the Z statistics also show a high level of overlap across the different damage levels. However, because all damages are detected under a wide range of alpha (false alarm) levels, the ROC plot in Figure 9c shows perfect detection for the first damage by the Z statistic, and also an almost perfect detection by the DI metric. Turning to Figure 9 panels b and d, one can observe the slightly-enhanced separation between the damage-specific Z statistic curves. In addition, the Z statistic shows superior detection capability once more over the DI for the first damage level, as shown in panel d of Figure 9.

Quantification: Results and Discussion

Unlike the case of the CFRP coupon, where the attached weights resembled a continuous growing crack, damage levels in the Al panel correspond to discrete classes of damage. Thus, the problem of quantification is addressed from a classification point of view, instead of regression. As such, in order to demonstrate the capability of Z-trained GP classification models, binary (that is, 2-class) models were trained using 80 single-frequency Z statistic values, in which the models are capable of classifying between two damage states/levels only. These models entertain simplicity and low computational burden, and can be used for comparing the healthy baseline or a known damage case with unknown test data. Figure 10 shows the first case, where the predictive probabilities are plotted against the values of the Z statistic used for prediction/classification at a frequency of 846 kHz for each case. As shown, the prediction probabilities in each case follow the validation points (dashed lines) not used in training very well. One advantage of this GP classification approach is the direct extraction of prediction probabilities without the need for any further computations, as in the case with damage

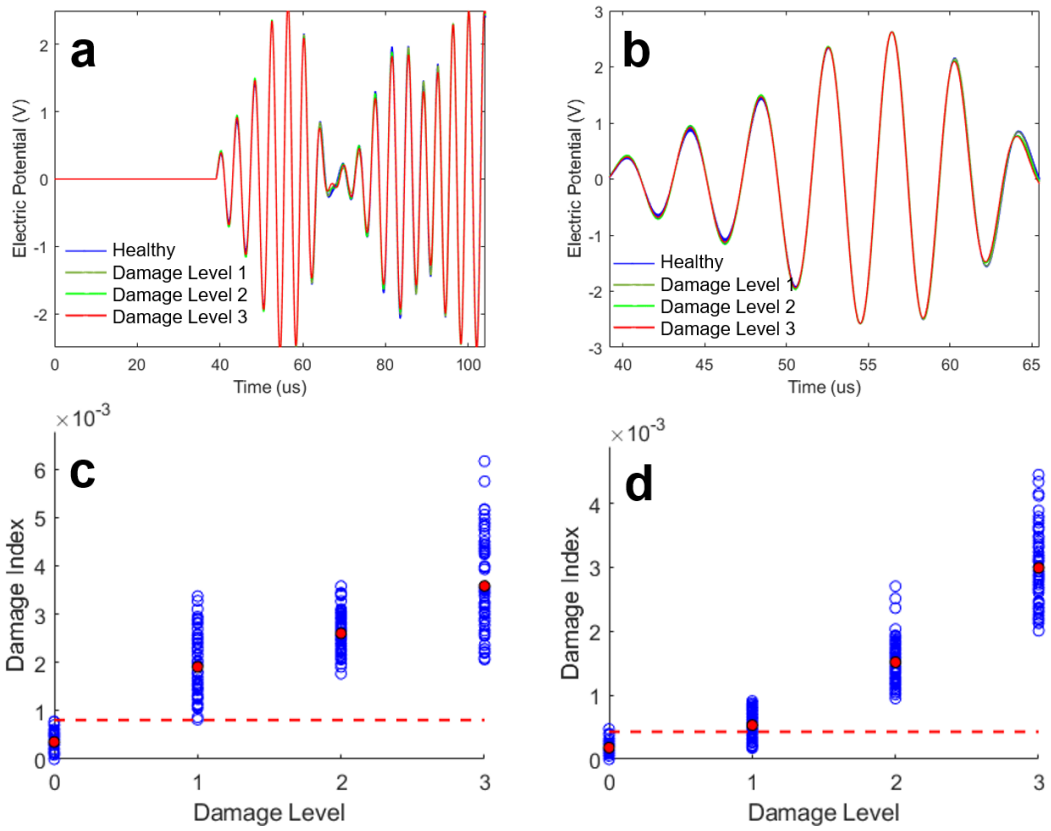

Fig. 8. Response signals from path 4-14 in the Al panel and their corresponding DIs for different damage levels. (a) and (c) present results for the first $100\mu s$ of the signal. (b) and (d) present results for the first $50\mu s$ of the signal. The red dashed lines indicate the upper 95 % confidence bound for the healthy DI values, while the red circles indicate the mean of all realizations per damage.

size prediction in GPRMs that was presented in the previous test case. In addition, the same probabilities can be extracted when comparing one of the known damage levels with the test data, which would add more insight into the most probable damage level of the test data. Finally, with an added computational burden, multi-label GP classification can be applied here to calculate the predictive probabilities corresponding to all damage levels simultaneously.

CONCLUSIONS

In this study, a unified probabilistic active-sensing SHM framework for damage detection and quantification was put forward using stochastic non-parametric time series and Bayesian Gaussian Process regression and classification models. The application of the framework was demonstrated on two representative test cases corresponding to modern-day rotorcraft materials/components. After selecting the most damage-informative signal paths to be analyzed based on the postulated statistical path selection method, a novel damage sensitive Z statistic was proposed and applied to damage detection showing superiority over conventional damage indices in both test cases. Then, these statistics were used for training GP regression and classification models for the CFRP coupon and stiffened Al panel, respectively, for tackling the damage quantification and classificaiton tasks. Results showed excellent damage size prediction in the case of the CFRP coupon, and accurate damage level classification in the case of the Al stiffened panel. The presented experimental assessment and validation results indicated the potential advantages of using GP models for damage quantification and classification compared to conventional deterministic and arbitrary-threshold DI-based approaches. In conclusion, the proposed unified probabilistic active-sensing SHM framework exhibited accurate and robust damage detection and quantification performance in a data-efficient manner given the use of the proposed statistical path selection algorithm, thus outperforming alternative to conventional DI-based SHM metrics.

Author contact: Ahmad Amer, amera2@rpi.edu; Fotis Kopsaftopoulos, kopsaf@rpi.edu

ACKNOWLEDGMENTS

This work is carried out at the Rensselaer Polytechnic Institute under the Army/Navy/NASA Vertical Lift Research Center of Excellence (VLRCOE) Program, grant number W911W61120012, with Dr. Mahendra Bhagwat and Dr. William Lewis as Technical Monitors.

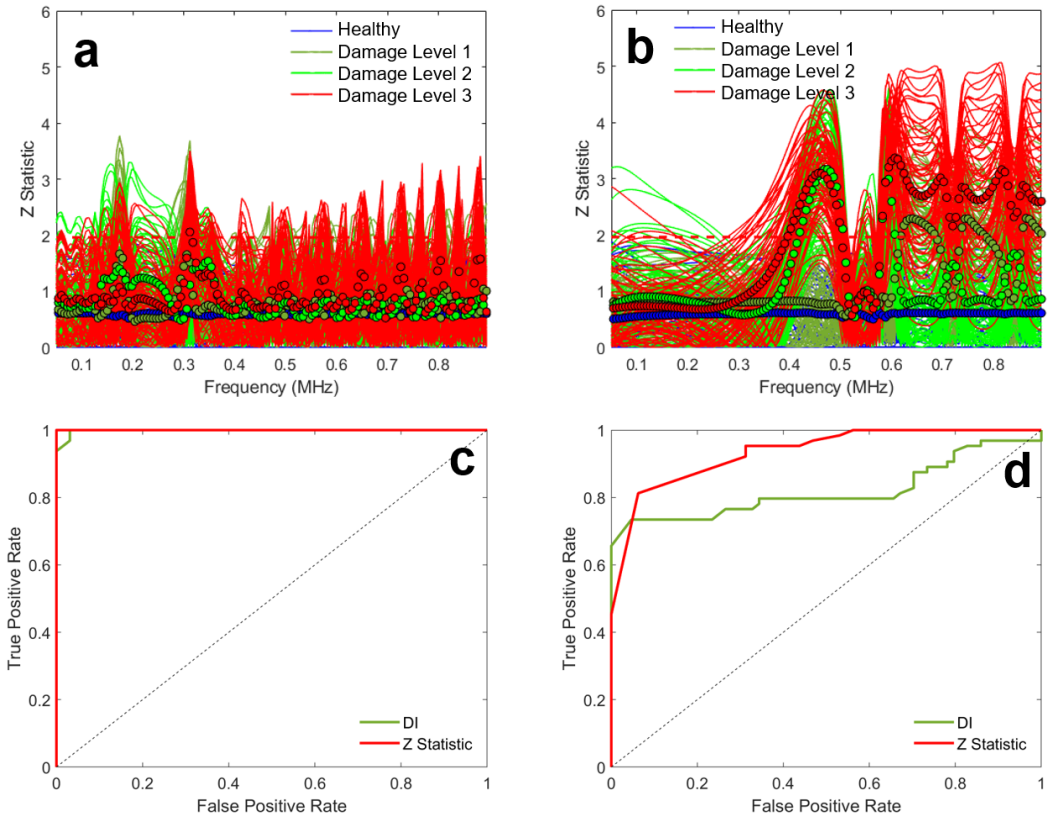

Fig. 9. NP-TS model results from path 4-14 in the Al panel for different damage levels. (a) Z Statistic for the first $100\mu s$. (b) Z Statistic for the first $50\mu s$. The red dashed lines indicate the upper 95 % confidence bound for the healthy Z statistics, and the colored circles indicate the mean Z value of all realizations per damage. Also shown are the ROC plots comparing Z statistics and DIs with respect to detecting the first damage size (1 weight) for (a) the first $100\mu s$ of the signal, and (d) first $50\mu s$ of the signal.

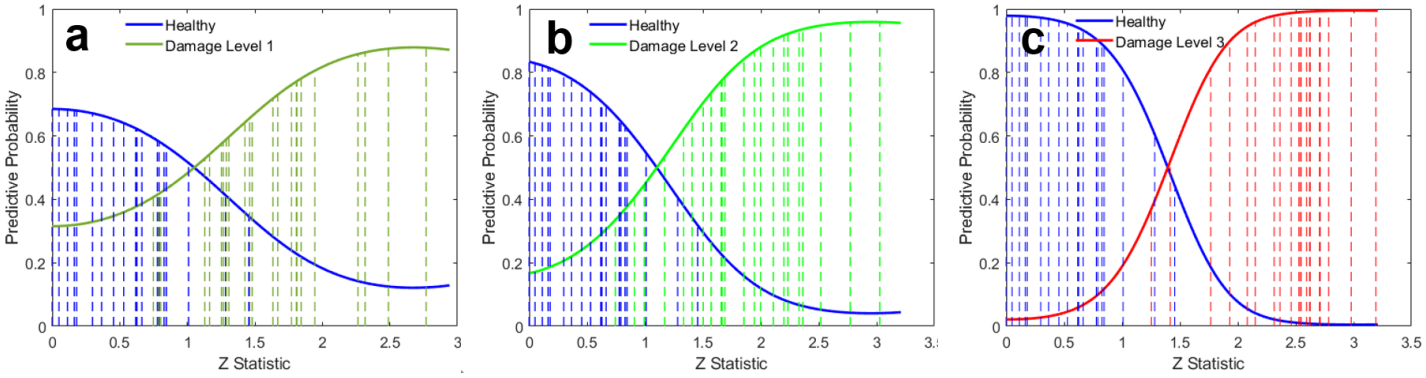

Fig. 10. Predictive probabilities from binary GP classification models trained by the Z statistics for a frequency of 846 kHz applied to the first $50\mu s$ of the response signal from path 4-14 in the Al panel. (a) Healthy *vs* Damage Level 1. (b) Healthy *vs* Damage Level 2. (c) Healthy *vs* Damage Level 3. The colored dashed lines correspond to validation (test) points that were not used in training the models for each structural state.

REFERENCES

[1]Kopsaftopoulos, F., Nardari, R., Li, Y.-H., and Chang, F.-K., "A stochastic global identification framework for aerospace structures operating under varying flight states," *Mechanical Systems and Signal Processing*, Vol. 98, 2018, pp. 425–447.
doi: 10.1016/j.ymssp.2017.05.001

[2]Poulimenos, A. G., *Modeling of non-stationary vibration*

signals via Functional Series (FS) TARMA models, Ph.D. thesis, Department of Mechanical Engineering and Aeronautics, University of Patras, Greece, 2007.

[3]Janapati, V., Kopsaftopoulos, F., Li, F., Lee, S., and Chang, F.-K., "Damage detection sensitivity characterization of acousto-ultrasound-based structural health monitoring techniques," *Structural Health Monitoring*, Vol. 15, (2), 2016, pp. 143–161.

[4]Ahmed, S. and Kopsaftopoulos, F. P., "Uncertainty quantification of guided waves propagation for active sensing structural health monitoring," Proceedings of the Vertical Flight Society 75th Annual Forum & Technology Display, May 2019.

[5]Wilson, C. L., Lonkar, K., Roy, S., Kopsaftopoulos, F., and Chang, F.-K., "Structural Health Monitoring of Composites," *Comprehensive Composite Materials II*, edited by P. W. R. Beaumont and C. H. Zweben, Elsevier Ltd., 2018, pp. 382–407.

[6]Ihn, J. and Chang, F.-K., "Pitch-catch active sensing methods in structural health monitoring for aircraft structures," *Structural Health Monitoring*, Vol. 7, (1), 2008, pp. 5–19.

[7]Giurgiutiu, V., "Piezoelectric Wafer Active Sensors for Structural Health Monitoring of Composite Structures Using Tuned Guided Waves," *Journal of Engineering Materials and Technology*, Vol. 133, (4), 2011, pp. 041012.

[8]Jin, H., Yan, J., Li, W., and Qing, X., "Monitoring of fatigue crack propagation by damage index of ultrasonic guided waves calculated by various acoustic features," *Applied Sciences*, Vol. 9, 2019, pp. 4254.

[9]Xu, B., Zhang, T., Song, G., and Gu, H., "Active interface debonding detection of a concrete-filled steel tube with piezoelectric technologies using wavelet packet analysis," *Mechanical Systems and Signal Processing*, Vol. 36, 2013, pp. 7–17.

[10]Nasrollahi, A., Deng, W., Ma, Z., and Rizzo, P., "Multimodal structural health monitoring based on active and passive sensing," *Structural Health Monitoring*, Vol. 17, (2), 2018, pp. 395–409.

[11]Lim, S. I., Cui, L., Liu, Y., and Soh, C. K., "Monitoring fatigue crack growth in narrow structural components using Lamb wave technique," Proc. SPIE 7981, Sensors and Smart Structures Technologies for Civil, Mechanical, and Aerospace Systems, April 2011.

[12]Soman, R., Malinowski, P., and Ostachowicz, W., "Comparative study of deterioration of composite due to moisture using strain, electro-mechanical impedence, and guided waves," Proc. SPIE 10600, Health Monitoring of Structural and Biological Systems XII, March 2018.

[13]Yan, J., Jin, H., Sun, H., and Qing, X., "Active monitoring of fatigue crack in the weld zone of Bogie frames using ultrasonic guided waves," *Sensors*, Vol. 19, 2019, pp. 3372.

[14]Dragan, K., Dziendzikowski, M., Klimaszewski, S., Klysz, S., and Kurnyta, A., "Energy correlated damage indices in fatigue crack extent quantification," *Key Engineering Materials*, Vol. 569–570, 2013, pp. 1186–1193.

[15]Farrar, C. R. and Worden, K., "An introduction to Structural Health Monitoring," *The Royal Society – Philosophical Transactions: Mathematical, Physical and Engineering Sciences*, Vol. 365, 2007, pp. 303–315.

[16]Spiridonakos, M. and Fassois, S., "Non-stationary random vibration modelling and analysis via functional series time-dependent ARMA (FS-TARMA) models–A critical survey," *Mechanical Systems and Signal Processing*, Vol. 47, (1-2), 2014, pp. 175–224.

[17]Zhang, Q. W., "Statistical damage identification for bridges using ambient vibration data," *Computers and Structures*, Vol. 85, 2007, pp. 476–485.

[18]Ahmed, S. and Kopsaftopoulos, F. P., "Investigation of broadband high-frequency stochastic actuation for active-sensing SHM under varying temperature," Proceedings of the 12th International Workshop on Structural Health Monitoring (IWSHM 2019), September 2019.

[19]Qiu, L., Yuan, S., Bao, Q., Mei, H., and Ren, Y., "Crack propagation monitoring in a full-scale aircraft fatigue test based on guided wave Gaussian mixture model," *Smart Materials and Structures*, Vol. 25, 2016, pp. 055048.

[20]Wang, F., Huo, L., and Song, G., "A piezoelectric active sensing method for quantitative monitoring of bolt loosening using energy dissipation caused by tangential damping based on the fractal contact theory," *Smart Materials and Structures*, Vol. 27, 2018, pp. 015023.

[21]Castro, E., Moreno-Garcia, P., and Gallego, A., "Damage Detection in CFRP Plates Using Spectral Entropy," *Shock and Vibration*, 2014, pp. 1–8.

[22]An, Y.-K., Giurgiutiu, V., and Sohn, H., "Integrated impedance and guided-wave-based damage detection," *Mechanical Systems and Signal Processing*, Vol. 28, 2012, pp. 50–62.

[23]Su, Z., Zhou, C., Hong, M., Cheng, L., Wang, Q., and Qing, X., "Acousto-ultrasonics-based fatigue damage characterization: linear versus nonlinear signal features," *Mechanical Systems and Signal Processing*, Vol. 45, 2014, pp. 225–239.

[24]Lize, E., Rebillat, M., Mechbal, N., and Bolzmacher, C., "Optimal dual-PZT and network design for baseline-free SHM of complex anisotropic composite structures," *Smart Materials and Structures*, Vol. 27, 2018, pp. 115018.

[25]Amer, A. and Kopsaftopoulos, F. P., "Probabilistic Damage Quantification *via* the Integration of Non-parametric Time-series and Gaussian Process Regression Models," Proceedings of the 12th International Workshop on Structural Health Monitoring (IWSHM 2019), September 2019.

[26]Qiu, J., Li, F., Abbas, S., and Zhu, Y., "A baseline-free damage detection approach based on distance compensation of guided waves," *Journal of Low Frequency, Vibration and Active Control*, Vol. 38, 2019, pp. 1132–1148.

[27]Hua, J., Cao, X., Yi, Y., and Lin, J., "Time-frequency damage index of broadband lamb wave for corrosion inspection," *Journal of Sound and Vibration*, Vol. 464, 2020, pp. 114985.

[28]Patra, S. and Banerjee, S., "Material State Awareness for Composites Part I: Precursor Damage Analysis Using Ultrasonic Guided Coda Wave Interferometry (CWI)," *Materials*, Vol. 10, 2017, pp. 1436.

[29]Amjad, U., Yadav, S. K., and Kundu, T., "Detection and quantification of delamination in laminated plates from the phase of appropriate guided wave modes," *Optical Engineering*, Vol. 55, (1), 2016, pp. 011006.

[30]Das, S., Kyriakides, I., Chattopadhyay, A., and Papandreou-Suppappola, A., "Monte Carlo matching pursuit decomposition method for damage quantification in composite structures," *Journal of Intelligent Materials Systems and Structures*, Vol. 20, 2009, pp. 647–658.

[31]Rizzo, P. and di Scalea, F. L., "Wavelet coefficient analysis for quantitative determination of damage in tendons and cables," Proc. SPIE 5765, Smart Structures and Materials, Sensors and Smart Structures Technologies for Civil, Mechanical, and Aerospace Systems, May 2005.

[32]Rizzo, P., Cammarata, M., Dutta, D., Sohn, H., and Harries, K., "An unsupervised learning algorithm for fatigue crack detection in waveguides," *Smart Materials and Structures*, Vol. 18, 2009, pp. 025016 (11pp).

[33]Wang, Z., Wei, L., and Cao, M., "Damage quantification with embedded piezoelectric aggregates based on wavelet packet energy analysis," *Sensors*, Vol. 19, 2019, pp. 425.

[34]Banerjee, S. and Ahmed, R., "Precursor/Incubation of multi-scale damage state quantification in composite materials: using hybrid microcontinuum field theory and high-frequency ultrasonics," *IEEE Transactions on Ultrasonics, Ferroelectrics and Frequency Control*, Vol. 60, (6), 2013, pp. 1141–1151.

[35]Borkowski, L. and Chattopadhyay, A., "Electromagnetomechanical elastodynamic model for Lamb wave damage quantification in composites," Proc. SPIE 9064, Health Monitoring of Structural and Biological Systems, March 2014.

[36]Banerjee, S. and Ahmed, R., "Quantitative structural health monitoring by ultrasonic guided waves," *Journal of Engineering Mechanics*, Vol. 136, (8), 2010, pp. 937–944.

[37]Zhao, J., Gao, H. D., Chang, G. F., Ayhan, B., Yan, F., Kwan, C., and Rose, J. L., "Active health monitoring of an aircraft wing with embedded piezoelectric sensor/actuator network: I. Defect detection, localization and growth monitoring," *Smart Materials and Structures*, Vol. 16, (4), 2007, pp. 1208–1217.

[38]Flynn, E. B., Todd, M. D., Wilcox, P. D., Drinkwater, B. W., Croxford, A. J., and Kessler, S., "Maximum-likelihood estimation of damage location in guided-wave structural health monitoring," *Proceedings of The Royal Society A, Burlington, VT*, Vol. 467, (2133), 2011, pp. 2575–2596.

[39]Todd, M. D., Flynn, E. B., Wilcox, P. D., Drinkwater, B. W., Croxford, A. J., and Kessler, S., "Ultrasonic wave-based defect localization using probabilistic modeling," American Institute of Physics Conference Proceedings, May 2012.

[40]Haynes, C., Todd, M., Flynn, E., and Croxford, A., "Statistically-based damage detection in geometrically-complex structures using ultrasonic interrogation," *Structural Health Monitoring*, Vol. 12, (2), 2012, pp. 141–152.

[41]Ng, C.-T., "On the selection of advanced signal processing techniques for guided wave damage identification using a statistical approach," *Engineering Structures*, Vol. 67, 2014, pp. 50–60.

[42]Mujica, L. E., Ruiz, M., Pozo, F., Rodellar, J., and Güemes, A., "A structural damage detection indicator based on principal component analysis and statistical hypothesis testing," *Smart Materials and Structures*, Vol. 23, (2), dec 2013, pp. 025014.
doi: 10.1088/0964-1726/23/2/025014

[43]Amer, A. and Kopsaftopoulos, F. P., "Probabilistic active sensing acousto-ultrasound SHM based on non-parametric stochastic representations," Proceedings of the Vertical Flight Society 75th Annual Forum & Technology Display, May 2019.

[44]Su, Z. and Ye, L., "Lamb wave-based quantitative identification of delamination in CF/EP composite structures using artificial neural algorithm," *Composite Structures*, Vol. 66, 2004, pp. 627–637.

[45]Song, G., Gu, H., and Mo, Y.-L., "Smart aggregates: multi-functional sensors for concrete structure —a tutorial and a review," *Smart Materials and Structures*, Vol. 17, 2008, pp. 033001.

[46]Tibaduiza, D. A., Mujica, L. E., Rodellar, J., and Güemes, A., "Structural damage detection using principal component analysis and damage indices," *Journal of Intelligent Material Systems and Structures*, Vol. 27, (2), 2016, pp. 233–248.

[47]Peng, T., Saxena, A., Goebel, K., Xiang, Y., Sankararaman, S., and Liu, Y., "A novel Bayesian imaging method for probabilistic delamination detection of composite materials," *Smart Materials and Structures*, Vol. 22, 2013, pp. 125019–125028.

[48]Yang, J., He, J., Guan, X., Wang, D., Chen, H., Zhang, W., and Liu, Y., "A probabilistic crack size quantification method using in-situ Lamb wave test and Bayesian updating," *Mechanical Systems and Signal Processing*, Vol. 78, 2016, pp. 118–133.

[49]He, J., Ran, Y., Liu, B., Yang, J., and Guan, X., "A Lamb wave based fatigue crack length estimation method using finite element simulations," The 9th International Symposium on NDT in Aerospace, Xiamen, China, November 2017.

[50]Kopsaftopoulos, F. P. and Fassois, S. D., "Experimental assessment of time series methods for structural health monitoring (SHM)," Proceedings of the 4th European Workshop on Structural Health Monitoring (EWSHM), 2008.

[51]Kopsaftopoulos, F. P. and Fassois, S. D., "Vibration Based Health Monitoring for a Thin Aluminum Plate – A Comparative Assessment of Statistical Time Series Methods," Proceedings of the 5th European Workshop on Structural Health Monitoring (EWSHM), 2010.

[52]Kopsaftopoulos, F. P. and Fassois, S. D., "Vibration based health monitoring for a lightweight truss structure: experimental assessment of several statistical time series methods," *Mechanical Systems and Signal Processing*, Vol. 24, 2010, pp. 1977–1997.

[53]Fassois, S. D. and Kopsaftopoulos, F. P., "Statistical Time Series Methods for Vibration Based Structural Health Monitoring," *New Trends in Structural Health Monitoring*, edited by W. Ostachowicz and A. Guemes, Chap. 4, Springer, 2013, pp. 209–264.

[54]Kopsaftopoulos, F. and Fassois, S. D., "Vibration based health monitoring for a lightweight truss structure: experimental assessment of several statistical time series methods," *Mechanical Systems and Signal Processing*, Vol. 24, 2010, pp. 1977–1997.

[55]Kopsaftopoulos, F. P. and Fassois, S. D., "A Functional Model Based Statistical Time Series Method for Vibration Based Damage Detection, Localization, and Magnitude Estimation," *Mechanical Systems and Signal Processing*, Vol. 39, 2013, pp. 143–161.
doi: 10.1016/j.ymssp.2012.08.023

[56]Kopsaftopoulos, F. P. and Fassois, S. D., "Identification of Stochastic Systems Under Multiple Operating Conditions: The Vector-dependent Functionally Pooled (VFP) Parametrization," *under preparation for publication*, 2016.

[57]Ljung, L., *System Identification: Theory for the User*, Prentice–Hall, second edition, 1999.

[58]Kay, S. M., *Modern Spectral Estimation: Theory and Application*, Prentice Hall: New Jersey, 1988, p. 46.

[59]Manolakis, D., Ingle, V. K., and Kogon, S. M., *Statistical and Adaptive Signal Processing: Spectral Estimation, Signal Modeling, Adaptive Filtering and Array Processing*, Artech House, New York, 2005, pp. 225–255.

[60]Manasas, M., Jane, R., Fiz, G. A., Morera, J., and Caminal, P., "Influence of estimators of spectral density on the analysis of electromyographic and vibromyographic signals," *Medical and Biological Engineering and Computing*, Vol. 40, 2002, pp. 90–98.

[61]Hayes, M. H., *Statistical Digital Signal Processing and Modelling*, John Wiley and Sons, New York, 1996.

[62]Kolmogorov, A. N., "Confidence limits for an unknown distribution function," *Annals of Mathematical Statistics*, Vol. 12, 1941, pp. 461–463.

[63]Smirnoff, H., "Sur les Écarts de la Courbe de la Distribution Empirique," *Receuil Mathémathique (Matematiceskii Sbornik)*, Vol. 6, 1939, pp. 3–26.

[64]Engmann, S. and Cousineau, D., "Comparing distributions: The two-sample Anderson-Darling test as an alternative to the Kolmogorov Smirnoff test," *Journal of Applied Quantitative Methods*, Vol. 6, (3), 2011, pp. 1–17.

[65]Matlab®, *Two-sample Kolmogorov-Smirnov Test (R2019a)*.

[66]Massey, F. J., "The Kolmogorov-Smirnov test of goodness of fit," *Journal of The American Statistical Association*, Vol. 46, 1951, pp. 68–78.

[67]C. E. Rasmussen and C. K. I. Williams, editors, *Gaussian Processes for Machine Learning*, MIT Press, 2006.

[68]Rogers, T., Gardner, P., Dervilis, N., Worden, K., A.E., M., Papatheou, E., and Cross, E., "Probabilistic modelling of wind turbine power curves with application of heteroscedastic Gaussian process regression," *Renewable Energy*, Vol. 148, 2020, pp. 1124–1136.

[69]Ahmed, S., Amer, A., Varela, C., and Kopsaftopoulos, F. P., "Data Driven State Awareness for Fly-by-Feel Aerial Vehicles via Adaptive Time Series and Gaussian Process Regression Models," Proceedings of the InfoSymbiotics/DDDAS2020 Conference, 2020.